

From EMC- and Cronin-effects to signals of quark-gluon plasma

Wei Zhu¹, Jianhong Ruan¹ and Fengyao Hou²

¹Department of Physics, East China Normal University, Shanghai 200062, P.R. China

²Kavli Institute for Theoretical Physics China(KITPC),
Institute of Theoretical Physics, CAS, Beijing 100190, P.R. China

Abstract

The EMC- and Cronin-effects are explained by a unitarized evolution equation, in which the shadowing and antishadowing corrections are dynamically produced due to gluon fusions. For this sake, an alternative form of the GLR-MQ-ZRS equation is derived. The resulting gluon distributions, integrated and unintegrated, in protons and nuclei are used for analysis of the contributions of the initial parton distributions to the nuclear suppression factor in heavy ion collisions. A simulation of the fractional energy loss is extracted from the data of RHIC and LHC, where the contributions of both nuclear shadowing and nuclear antishadowing effects are considered. We find a rapid crossover from weak energy loss to strong energy loss with the gluon jet at a universal critical energy, $E_c \sim 10\text{GeV}$.

PACS number(s): 24.85.+p; 12.38.-t; 13.60.Hb

keywords: Quark gluon plasma; Nuclear gluon distribution; Energy loss

1 Introduction

One of the important findings at RHIC and LHC is that the hadron production at high transverse momentum k_t in central heavy ion collisions is suppressed when compared to the one in p+p collisions [1, 2]. This suppression can be attributed to energy loss of high- k_t partons that transverse the hot and dense medium (i.e., quark-gluon plasma QGP) produced in those collisions. An important goal of the study of heavy ion collisions is therefore to determine the properties of QGP by measuring the fractional energy loss where the nuclear effects on the initial parton distributions should be subtracted.

The parton densities in a bound nucleon differ from those in a free one. One example is that the ratio of nuclear structure functions to deuterium's is smaller or larger than unity at Bjorken variable $x < 0.1$ or $0.1 < x < 0.3$. These two facts are called as the nuclear shadowing and antishadowing in the EMC effect [3]. The nuclear shadowing and antishadowing effects originate from the gluon fusion and recombination between two different nucleons in a nucleus, which will change the distributions of gluon and quarks but not their total momentum [4]. In consequence, the loss of gluon momentum in the shadowing range should be compensated by the momentum of new gluons at larger x , which is named the antishadowing effect.

Another example is the Cronin effect: the ratio of particle yields in $d + A$ (scaled by the number of collisions) to those in $p + p$, is over or under unity in an intermediate transverse momentum range (Cronin enhancement) or in a smaller transverse momentum range (anti-Cronin suppression). This effect was first found at lower fixed target energies [5] and then was confirmed in $d + Au$ collisions at the BNL Relativistic Heavy Ion Collider (RHIC)(where $\sqrt{s} = 200 GeV$) [6-9].

The Cronin effect is more complicated than the EMC effect. The former mixes the shadowing-antishadowing corrections at initial state and the medium modifications at

final state. The later provides important information for understanding the properties of dense and hot matter formed in high-energy heavy-ion collisions. Therefore, the nuclear shadowing and antishadowing effects, which appear in the EMC effect, should be extracted from the Cronin effect to exposes the properties of the medium.

The saturation models are broadly used to study the Cronin effect. The saturation is a limiting behavior of the shadowed gluon distribution in the Jalilian-Marian-Iancu-McLerran-Weigert-Leonidov-Kovner (JIMWLK) equation [10-15], where the unintegrated gluon distribution is flat in k_t -space when k_t is smaller than the saturation scale Q_s . An elementary QCD process, which also causes nonlinear corrections in the JIMWLK equation, is the gluon fusion $gg \rightarrow g$. As we have mentioned before, the antishadowing effect always coexists with the shadowing effect in *any gluon fusion processes* due to a general restriction of momentum conservation [16-18]. However, such antishadowing effect is completely neglected in the original saturation models. The Cronin enhancement in these models, (i) is additionally explained as multiple scattering [19-22] using the Glauber-Mueller model [23] or the McLerran-Venugopalan model [24,25]; (ii) is produced by special initial gluon distributions of proton and nucleus [26]. A question is then followed: How much does the nuclear antishadowing effect contribute to the Cronin effect?

A global Dokshitzer-Gribov-Lipatov-Altarelli-Parisi (DGLAP) analysis of nuclear parton distribution functions (for example, the ESP09-set [27,28]) was proposed. In the DGLAP analysis, the data of Drell-Yan dilepton production from deep inelastic scattering (DIS), and the data of inclusive high- k_t hadron production measured at RHIC are used. It is found that a strong gluon antishadowing effect is necessary to support the data at RHIC. Since the DGLAP equation [29-31] does not contain the nonlinear corrections of gluon fusion, the shadowing and antishadowing effects in the DGLAP analysis are phenomenologically adopted as initial conditions. However, this brings about un-

certainty due to the lack of the experimental data about nuclear gluon distribution. A similar global DGLAP analysis shows that the available data are not enough to fix all the complicated input distributions and that it isn't sure whether the antishadowing effect does appear or not[32,33]. Besides, the DGLAP equation in the collinear factorization scheme evolves the integrated parton distributions. The behavior of the unintegrated gluon distributions, which contain information of the transverse momentum distribution, is completely unknown in the DGLAP scheme. Therefore, the ESP09-set of nuclear parton distributions can't predict with good accuracy the data at lower k_t at RHIC, where the contributions from intrinsic transverse momentum become more important [27,28].

The modification of the gluon recombination to the standard DGLAP evolution equation was first proposed by Gribov-Levin-Ryskin and Mueller-Qiu (the GLR-MQ equation) in [34,35]. This GLR-MQ equation is naturally regarded as a better scheme to describe the QCD dynamics of the nuclear shadowing since the same gluon fusion exists both in proton and in nucleus but differs in the strength of the nonlinear terms [36,37]. However, the GLR-MQ equation can't predict the nuclear antishadowing effect due to it violates the momentum conservation. This defect is remedied by a modified equation (the GLR-MQ-ZRS equation) proposed by Zhu, Ruan and Shen in their works[38-40], where the corrections of the gluon fusion to the DGLAP equation lead to both shadowing and antishadowing effects. Although, the integral solutions of the GLR-like equations in present need the initial distributions on a boundary line (x, Q_0^2) at a fixed Q_0^2 , and the unknown input with nuclear shadowing and antishadowing effects at small x still exist.

This work tries to improve the GLR-like methods motioned above. We study the nuclear shadowing and antishadowing effects in the EMC- and Cronin-effects, which are dynamically arisen from the gluon recombination. Then we use the resulting nuclear gluon distributions to produce the contributions of the initial parton distributions to the

nuclear suppression factor in heavy ion collisions and to extract fractional energy loss from the data in RHIC and in LHC. For this sake, an alternative form of the GLR-MQ-ZRS equation at the double-leading-logarithmic-approximation (DLLA) is derived in Sec. 2. This equation will evolve along small x -direction. The nonlinear corrections to the input distributions can be neglected if the value of the starting point x_0 is large enough. Both the shadowing and antishadowing effects are naturally grown up with the evolution of x along the direction from x_0 to smaller x . This scheme avoids the non-perturbative nuclear modifications to the input distributions and then simplifies the initial conditions. The existing data about the EMC- and Cronin-effects is used to fix a few of free parameters in the solutions. Then the integrated and unintegrated gluon distributions in proton and nuclei are obtained to analyze the nuclear suppression factor in heavy ion collisions.

Our main conclusions are: (i) we support the stronger shadowing-antishadowing effects both in the unintegrated and integrated gluon distributions due to a strong A -dependence of the nonlinear corrections in the heavy nucleus; (ii) both the anti-Cronin suppression and Cronin enhancement mainly originate from the same gluon recombination mechanism in the nuclear shadowing and antishadowing effects of the EMC effect; (iii) fractional energy loss is rapidly crossover from weak energy loss to strong energy loss with the gluon jet at a universal critical energy, $E_c \sim 10 GeV$.

This work is organized as follows. We derive the GLR-MQ-ZRS equation in a new form in Sec.2. Basing on this equation we study the shadowing and antishadowing effects in the EMC effect in Sec.3. The nuclear shadowing and antishadowing contributions to the Cronin effect are exposed by using the resulting unintegrated gluon distributions in proton and nuclei in Sec.4. The nuclear shadowing and antishadowing effects to the nuclear suppression factor are predicted and a simulations of fractional energy loss is extracted from the data at RHIC and at LHC in Sec. 5.

2 A new form of the GLR-MQ-ZRS equation

In history, the DGLAP evolution equation is derived by using the renormalization group method for the integrated distributions. The resulting equation evolves with factorization scale μ . In this section, we try to rewrite the DGLAP equation with the nonlinear modifications beginning from the unintegrated distributions. Then, we get an alternative form of the equation, which evolves the Bjorken variable x .

We begin from a deep inelastic scattering process, where the unintegrated gluon distribution is measured. In the k_t -factorization scheme, the cross section is decomposed into

$$\begin{aligned}
 & d\sigma(\text{probe}^*P \rightarrow kX) \\
 &= f(x_1, k_{1t}^2) \otimes \mathcal{K} \left(\frac{k_t^2}{k_{1t}^2}, \frac{x}{x_1}, \alpha_s \right) \otimes d\sigma(\text{probe}^*k_1 \rightarrow k) \\
 &\equiv \Delta f(x, k_t^2) \otimes d\sigma(\text{probe}^*k_1 \rightarrow k),
 \end{aligned} \tag{1}$$

which contains the evolution kernel \mathcal{K} , the unintegrated gluon distribution function f and the probe^* -parton cross section $d\sigma(\text{probe}^*k_1 \rightarrow k)$. For simplicity, we fix the QCD coupling at the leading order (LO) approximation in this work. According to the scale-invariant parton picture of the renormalization group [41], we regard $\Delta f(x, k_t^2)$ as the increment of the distribution $f(x_1, k_{1t}^2)$ when it evolves from (x_1, k_{1t}^2) to (x, k_t^2) . Thus, the connection between $f(x_1, k_{1t}^2)$ and $f(x, k_t^2)$ via Eq. (1) is

$$\begin{aligned}
 & f(x, k_t^2) = f(x_1, k_{1t}^2) + \Delta f(x, k_t^2) \\
 &= f(x_1, k_{1t}^2) + \int_{k_{1t, \min}^2}^{k_t^2} \frac{dk_{1t}^2}{k_{1t}^2} \int_x^1 \frac{dx_1}{x_1} \mathcal{K} \left(\frac{k_t^2}{k_{1t}^2}, \frac{x}{x_1}, \alpha_s \right) f(x_1, k_{1t}^2).
 \end{aligned} \tag{2}$$

In the case of the LO DGLAP evolution, we adopt a physical gauge(axial gauge), in which only the transverse gluon polarizations are summed over, so that the ladder-type diagrams

dominate the evolution. The unintegrated distributions satisfy the normalization relation

$$G(x, \mu^2) \equiv xg(x, \mu^2) = \int_{k_{t,min}^2}^{\mu^2} \frac{dk_t^2}{k_t^2} x f(x, k_t^2) \equiv \int_{k_{t,min}^2}^{\mu^2} \frac{dk_t^2}{k_t^2} F(x, k_t^2), \quad (3)$$

where the possible non-logarithmic tail when $k_t > \mu$ are beyond NLO accuracy. These distributions correspond to the density of partons in the proton with longitudinal momentum fraction x with the parton transverse momentum integrated up to $k_t = \mu$.

From Eqs. (2) and (3), we have

$$\Delta g(x, \mu^2) = \int_{k_{t,min}^2}^{\mu^2} \frac{dk_t^2}{k_t^2} \int_{k_{1t,min}^2}^{k_t^2} \frac{dk_{1t}^2}{k_{1t}^2} \int_x^1 \frac{dx_1}{x_1} \frac{1}{x_1} \mathcal{K} \left(\frac{k_t^2}{k_{1t}^2}, \frac{x}{x_1}, \alpha_s \right) F(x_1, k_{1t}^2), \quad (4)$$

or

$$\begin{aligned} \Delta G(x, \mu^2) &= \Delta xg(x, \mu^2) = \int_{k_{T,min}^2}^{\mu^2} \frac{dk_t^2}{k_t^2} \int_{k_{1t,min}^2}^{k_t^2} \frac{dk_{1t}^2}{k_{1t}^2} \int_x^1 \frac{dx_1}{x_1} \frac{x}{x_1} \mathcal{K} \left(\frac{k_t^2}{k_{1t}^2}, \frac{x}{x_1}, \alpha_s \right) F(x_1, k_{1t}^2) \\ &= \int_{k_{t,min}^2}^{\mu^2} \frac{dk_t^2}{k_t^2} \int_x^1 \frac{dx_1}{x_1} \frac{x}{x_1} \mathcal{K} \left(\frac{x}{x_1}, \alpha_s \right) G(x_1, k_t^2), \end{aligned} \quad (5)$$

where the last step is valid when the k_t is strongly ordered. Usually DGLAP evolution equation is written with the virtuality μ^2 rather than with k_t^2 , but at LO level the equation is the same with these two different arguments since the difference between them is a NLO effect. Therefore, we take

$$G(x, k_t^2) \rightarrow G(x, \mu^2). \quad (6)$$

Thus, in

$$G(x, \mu^2) = G(x_1, \mu_1^2) + \Delta G(x, \mu^2), \quad (7)$$

we write

$$\begin{aligned}
& \Delta G(x, \mu^2) \\
&= \int_{\mu_{1,min}^2}^{\mu^2} \frac{d\mu_1^2}{\mu_1^2} \int_x^1 \frac{dx_1}{x_1} \frac{x}{x_1} \mathcal{K}_{DGLAP}^{LL(\mu^2)}\left(\frac{x}{x_1}, \alpha_s\right) G(x_1, \mu_1^2), \tag{8}
\end{aligned}$$

at the leading logarithmic μ^2 approximation, in which the unregularized splitting kernel

$$\begin{aligned}
\frac{dx_1}{x_1} \mathcal{K}_{DGLAP}^{LL(\mu^2)} &= \frac{\alpha_s N_c}{\pi} \frac{dx_1}{x_1} \left[z(1-z) + \frac{1-z}{z} + \frac{z}{1-z} \right] \\
&= \frac{\alpha_s N_c}{\pi} \frac{dx_1}{x_1} \left[\frac{x(x_1-x)}{x_1^2} + \frac{x_1-x}{x} + \frac{x}{x_1-x} \right] \tag{9a}
\end{aligned}$$

$$\begin{aligned}
&\xrightarrow{x \ll x_1} \frac{dx_1}{x_1} \mathcal{K}_{DGLAP}^{DLL} = \frac{\alpha_s N_c}{\pi} \frac{dx_1}{x}. \tag{9b}
\end{aligned}$$

We add the contributions of the nonlinear recombination terms in Eq. (8) according to Refs. [38-40] (See Appendix),

$$\begin{aligned}
& \Delta G(x, \mu^2) \\
&= \int_{\mu_{1,min}^2}^{\mu^2} \frac{d\mu_1^2}{\mu_1^2} \int_x^1 \frac{dx_1}{x_1} \frac{x}{x_1} \mathcal{K}_{DGLAP}^{LL(\mu^2)}\left(\frac{x}{x_1}, \alpha_s\right) G(x_1, \mu_1^2) \\
&- 2 \int_{\mu_{1,min}^2}^{Q^2} \frac{d\mu_1^2}{\mu_1^4} \int_x^{1/2} \frac{dx_1}{x_1} \frac{x}{x_1} \mathcal{K}_{GLR-MQ-ZRS}^{GG \rightarrow GG, LL(\mu^2)}\left(\frac{x}{x_1}, \alpha_s\right) G^{(2)}(x_1, \mu_1^2) \\
&+ \int_{\mu_{1,min}^2}^{\mu^2} \frac{d\mu_1^2}{\mu_1^4} \int_{x/2}^{1/2} \frac{dx_1}{x_1} \frac{x}{x_1} \mathcal{K}_{GLR-MQ-ZRS}^{GG \rightarrow GG, LL(\mu^2)}\left(\frac{x}{x_1}, \alpha_s\right) G^{(2)}(x_1, \mu_1^2), \tag{10}
\end{aligned}$$

where

$$\begin{aligned}
& \frac{dx_1}{x_1} \mathcal{K}_{GLR-MQ-ZRS}^{GG \rightarrow GG, LL(\mu^2)} \\
&= \frac{\alpha_s^2}{8} \frac{N_c^2}{N_c^2 - 1} \frac{(2x_1 - x)(72x_1^4 - 48x_1^3x + 140x_1^2x^2 - 116x_1x^3 + 29x^4)}{x_1^5 x} dx_1 \tag{11a}
\end{aligned}$$

$$\begin{aligned}
&\xrightarrow{x \ll x_1} \frac{dx_1}{x_1} \mathcal{K}_{GLR-MQ-ZRS}^{GG \rightarrow GG, DLL} = 18\alpha_s^2 \frac{N_c^2}{N_c^2 - 1} \frac{dx_1}{x}. \tag{11b}
\end{aligned}$$

$$G^{(2)}(x, \mu^2) = R_G G^2(x, \mu^2), \tag{12}$$

where $R_G = 1/(\pi R^2)$ is a correlation coefficient with the dimension $[L^{-2}]$, and R is the effective correlation length of two recombination gluons. One can easily get the GLR-MQ-ZRS equation at DLL approximation

$$\begin{aligned} & \frac{\partial G(x, \mu^2)}{\partial \ln \mu^2} \\ &= \frac{\alpha_s N_c}{\pi} \int_x^1 \frac{dx_1}{x_1} G(x_1, \mu^2) - \frac{36\alpha_s^2}{\pi\mu^2 R^2} \frac{N_c^2}{N_c^2 - 1} \int_x^{1/2} \frac{dx_1}{x_1} G^2(x_1, \mu^2) \\ & \quad + \frac{18\alpha_s^2}{\pi\mu^2 R^2} \frac{N_c^2}{N_c^2 - 1} \int_{x/2}^{1/2} \frac{dx_1}{x_1} G^2(x_1, \mu^2). \end{aligned} \quad (13)$$

It is interesting to compare this small- x version of the GLR-MQ-ZRS equation with the GLR-MQ equation, which is [35]

$$\begin{aligned} & \frac{\partial G(x, \mu^2)}{\partial \ln \mu^2} \\ &= \frac{\alpha_s N_c}{\pi} \int_x^1 \frac{dx_1}{x_1} G(x_1, \mu^2) - \frac{36\alpha_s^2}{8\mu^2 R^2} \frac{N_c^2}{N_c^2 - 1} \int_x^{1/2} \frac{dx_1}{x_1} G^2(x_1, \mu^2), \end{aligned} \quad (14)$$

where

$$G^{(2)}(x, \mu^2) = \frac{9}{8\pi R^2} G^2(x, \mu^2), \quad (15)$$

is assumed.

Comparing with the GLR-MQ equation (14), there are several features in the GLR-MQ-ZRS equation (13): (i) the momentum conservation of partons is maintained; (ii) because of the shadowing and antishadowing effects in Eq. (13) have different kinematic regions, the net effect depends both on the local value of the gluon distribution at the observed point and on the shape of the gluon distribution when the Bjorken variable goes from x to $x/2$. In consequence, the shadowing effect in the evolution process will be obviously weakened more by the antishadowing effect if the distribution is steeper. Therefore, the antishadowing effect can not be neglected in the pre-saturation range.

According to the definition Eq. (3), one can roughly estimate the unintegrated gluon distribution using

$$F(x, k_t^2) \simeq \mu^2 \frac{\partial G(x, \mu^2)}{\partial \mu^2} \Big|_{\mu^2=k_t^2}. \quad (16)$$

However, Eq. (16) will be invalid with x increases, since the contribution of negative virtual DGLAP term will exceed the contribution of real emission one and lead to negative values of F . In fact, due to strong k_t ordered in DGLAP evolution, the transverse momentum of the final parton to leading-order is obtained just at the last step of the evolution. Thus, the k_t -dependent distribution can be calculated directly from the DGLAP equation if only keeping the contribution of a single real emission. Meanwhile, all the virtual contributions from the scale of k_t up to the final scale μ of the hard subprocess are resummed up into a Sudakov factor T , which describes the probability of no parton emission during the evolution. However, at the small x range, the virtual contributions to the gluon distribution in the DGLAP kernel can be neglected. We have indicated that the contributions of the virtual processes in the nonlinear kernels of the GLR-MQ-ZRS equation are canceled [38], therefore, the Sudakov form factors in nucleon are the same as those in nucleus[42] and can be canceled in their ratio. Thus, we use

$$\begin{aligned} & \Delta G(x, \mu^2) \\ &= \int_{k_{min}^2}^{\mu^2} \frac{dk_t^2}{k_t^2} \int_{k_{1t,min}^2}^{k_t^2} \frac{dk_{1t}^2}{k_{1t}^2} \int_x^1 \frac{dx_1}{x_1} \frac{x}{x_1} \mathcal{K}_{DGLAP}^{DLL} \left(\frac{x}{x_1}, \alpha_s \right) F(x_1, k_{1t}^2) \\ & - 2 \int_{\mu_{1min}^2}^{\mu^2} \frac{dk_t^2}{k_t^4} \int_x^{1/2} \frac{dx_1}{x_1} \frac{x}{x_1} \mathcal{K}_{MD-DGLAP}^{DLL} \left(\frac{x}{x_1}, \alpha_s \right) G^{(2)}(x_1, k_t^2) \\ & + \int_{\mu_{1min}^2}^{\mu^2} \frac{dk_t^2}{k_t^4} \int_{x/2}^{1/2} \frac{dx_1}{x_1} \frac{x}{x_1} \mathcal{K}_{MD-DGLAP}^{DLL} \left(\frac{x}{x_1}, \alpha_s \right) G^{(2)}(x_1, k_t^2), \end{aligned} \quad (17)$$

and obtain

$$\begin{aligned}
\Delta F(x, k_t^2) &= \mu^2 \frac{\partial \Delta G(x, \mu^2)}{\partial \mu^2} \Big|_{\mu^2=k_t^2} \\
&= \frac{\alpha_s N_c}{\pi} \int_{k_{1t, \min}^2}^{k_t^2} \frac{dk_{1t}^2}{k_{1t}^2} \int_x^1 \frac{dx_1}{x_1} F(x_1, k_{1t}^2) \\
&\quad - \frac{36\alpha_s^2}{k_t^2} \frac{N_c^2}{N_c^2 - 1} \int_x^{1/2} \frac{dx_1}{x_1} G^{(2)}(x_1, k_t^2) \\
&\quad + \frac{18\alpha_s^2}{k_t^2} \frac{N_c^2}{N_c^2 - 1} \int_{x/2}^{1/2} \frac{dx_1}{x_1} G^{(2)}(x_1, k_t^2), \tag{18}
\end{aligned}$$

Now we re-derive the GLR-MQ-ZRS equation, which evolves with the longitudinal momentum now. We differentiate

$$F(x, k_t^2) = F(x_1, k_{1t}^2) + \Delta F(x, k_t^2), \tag{19}$$

with respect to x . Note that

$$\begin{aligned}
& - \frac{\partial F(x, k_t^2)}{\partial x} \\
&= \int_{k_{1t, \min}^2}^{k_t^2} \frac{dk_{1t}^2}{k_{1t}^2} \frac{1}{x_1} \mathcal{K} \left(\frac{k_t^2}{k_{1t}^2}, \frac{x}{x_1}, \alpha_s \right) F(x_1, k_{1t}^2) \Big|_{x_1=x} \\
&\quad - \int_{k_{1t, \min}^2}^{k_t^2} \frac{dk_{1t}^2}{k_{1t}^2} \int_x^1 \frac{dx_1}{x_1^2} \frac{\partial x \mathcal{K} \left(\frac{k_t^2}{k_{1t}^2}, \frac{x}{x_1}, \alpha_s \right)}{\partial x} F(x_1, k_{1t}^2). \tag{20}
\end{aligned}$$

Generally, the resummation solution is hard to be obtained from this equation. However, the second term on the right-hand side of Eq. (20) vanishes at the $LL(1/x)$ approximation. In this case, the resummation becomes simple, i.e., we have

$$\begin{aligned}
& -x \frac{\partial F(x, k_t^2)}{\partial x} \\
&= \frac{\alpha_s N_c}{\pi} \int_{k_{1t, \min}^2}^{k_t^2} \frac{dk_{1t}^2}{k_{1t}^2} F(x, k_{1t}^2) \\
& - \frac{36\alpha_s^2}{\pi R^2 k_t^2} \frac{N_c^2}{N_c^2 - 1} \left[\int_{k_{1t, \min}^2}^{k_t^2} \frac{dk_{1t}^2}{k_{1t}^2} F(x, k_{1t}^2) \right]^2 + \frac{18\alpha_s^2}{\pi R^2 k_t^2} \frac{N_c^2}{N_c^2 - 1} \left[\int_{k_{1t, \min}^2}^{k_t^2} \frac{dk_{1t}^2}{k_{1t}^2} F \left(\frac{x}{2}, k_{1t}^2 \right) \right]^2,
\end{aligned}$$

$$(x \leq 0.15);$$

$$\begin{aligned}
& -x \frac{\partial F(x, k_t^2)}{\partial x} \\
= & \frac{\alpha_s N_c}{\pi} \int_{k_{1t, \min}}^{k_t^2} \frac{dk_{1t}^2}{k_{1t}^2} F(x, k_{1t}^2) + \frac{18\alpha_s^2}{\pi R^2 k_t^2} \frac{N_c^2}{N_c^2 - 1} \left[\int_{k_{1t, \min}}^{k_t^2} \frac{dk_{1t}^2}{k_{1t}^2} F\left(\frac{x}{2}, k_{1t}^2\right) \right]^2, \quad (0.15 \leq x \leq 0.3),
\end{aligned} \tag{21}$$

This is a new form of the GRL-MQ-ZRS equation. The negative and positive nonlinear terms correspond to the shadowing and antishadowing effects in the gluon recombination. Here the shadowing and antishadowing coexist in the region $x \leq 0.15$, while only the antishadowing exists in $0.15 \leq x \leq 0.3$.

The kinematic regions of Eq. (21) can be explained as follows. The evolution kernel of the GLR-MQ-ZRS equation (11a) as same as the DGLAP equation (9a) is derived at LL(Q^2) approximation and valid in a whole x range. However the DLLA form of the GLR-MQ-ZRS equation (11b) is valid at the small x range when $x < x_1$, here $x_1 \sim \mathcal{O}(10^{-1})$ according to $\alpha_s \ln(1/x) \ln(k_T^2/\mu^2) \sim \mathcal{O}(1)$. We take $x_1 = 0.15$ in this work.

Now we apply Eq. (21) in the nuclear target. The Shadowing and antishadowing effects thought arise from a nonlinear mechanism when gluons are sufficiently dense to interact with themselves. The strength of the gluon recombination is proportional to the gluon density in the transverse area. The gluons with smaller x will exceed the longitudinal size of nucleon in a nucleus. Thus, the strength of the nonlinear recombination terms in Eq. (21) should be scaled by $A^{1/3}$ in a nucleus. On the other hand, although the softer gluons of different nucleons with extra small k_t maybe correlate with each other in the transverse area, we still neglect these corrections because the integrations on k_t can go down to a very small value in Eq. (21) and $F(x, k_t^2 \rightarrow 0) \rightarrow 0$. In this simple model, Eq. (21) in the nucleus becomes

$$-x \frac{\partial F_A(x, k_t^2)}{\partial x}$$

$$\begin{aligned}
&= \frac{\alpha_s N_c}{\pi} \int_{k_{1t, \min}^2}^{k_t^2} \frac{dk_{1t}^2}{k_{1t}^2} F_A(x, k_{1t}^2) \\
&- A^{1/3} \frac{36\alpha_s^2}{\pi R^2 k_t^2} \frac{N_c^2}{N_c^2 - 1} \left[\int_{k_{1t, \min}^2}^{k_t^2} \frac{dk_{1t}^2}{k_{1t}^2} F_A(x, k_{1t}^2) \right]^2 + A^{1/3} \frac{18\alpha_s^2}{\pi R^2 k_t^2} \frac{N_c^2}{N_c^2 - 1} \left[\int_{k_{1t, \min}^2}^{k_t^2} \frac{dk_{1t}^2}{k_{1t}^2} F_A\left(\frac{x}{2}, k_{1t}^2\right) \right]^2, \\
&\quad (10^{-2} \leq x \leq 0.15);
\end{aligned}$$

$$\begin{aligned}
&-x \frac{\partial F_A(x, k_t^2)}{\partial x} \\
&= \frac{\alpha_s N_c}{\pi} \int_{k_{1t, \min}^2}^{k_t^2} \frac{dk_{1t}^2}{k_{1t}^2} F_A(x, k_{1t}^2) + A^{1/3} \frac{18\alpha_s^2}{\pi R^2 k_t^2} \frac{N_c^2}{N_c^2 - 1} \left[\int_{k_{1t, \min}^2}^{k_t^2} \frac{dk_{1t}^2}{k_{1t}^2} F_A\left(\frac{x}{2}, k_{1t}^2\right) \right]^2, \quad (0.15 \leq x \leq 0.3), \\
&\quad (22)
\end{aligned}$$

The input gluons are distributed on the boundary line $(2x_0, k_t)$ at fixed $2x_0$. We take a larger value of x_0 as a starting point of the evolution, where the gluons just begin to fuse and the nonlinear corrections to the input gluon distributions can be neglected. Meanwhile the contributions of the Fermi motion and nuclear binding effects to the nuclear parton distributions at small x are small enough. In this case, a nucleus is composed simply with incoherent constituent nucleons at $2x_0$. we have

$$F(2x_0, k_t^2) = F_A(2x_0, k_t^2), \quad (23)$$

where the nuclear parton distributions have been normalized.

Although a pure DGLAP equation is used at very small x in some papers, we find the DGLAP equation with shadowing corrections Eq. (21) predicts a smaller F_2 than experiment data when $x < 10^{-3}$. In fact, the DGLAP kernel in Eq. (21) resums the leading $\alpha_s \ln(1/x) \ln(k_t^2/\mu^2)$ contributions doubly. As we know that the BFKL evolution [43-48] which resums the leading $\ln(1/x)$ contributions and should replace the DGLAP equation at very small x ($x < 10^{-3}$) according to $\alpha_s \ln(1/x) \sim \mathcal{O}(1)$. In this region, we write Eq. (2) as

$$\Delta f(x, k_t^2) = \int_{k_{1t, \min}^2}^{\infty} \frac{d^2 \mathbf{k}_{1t}}{k_{1t}^2} \int_x^1 \frac{dx_1}{x_1} \mathcal{K} \left(\frac{k_t^2}{k_{1t}^2}, \frac{x}{x_1}, \alpha_s \right) f(x_1, k_{1t}^2), \quad (24)$$

or

$$\Delta F(x, k_t^2) = \int_{k_{1t, \min}^2}^{\infty} \frac{d^2 \mathbf{k}_{1t}}{k_{1t}^2} \int_x^1 \frac{dx_1}{x_1} \frac{x}{x_1} \mathcal{K} \left(\frac{k_t^2}{k_{1t}^2}, \frac{x}{x_1}, \alpha_s \right) F(x_1, k_{1t}^2), \quad (25)$$

where

$$F(x, k_t^2) = F(x_1, k_{1t}^2) + \Delta F(x, k_t^2), \quad (26)$$

and

$$\frac{x}{x_1} \mathcal{K} \left(\frac{k_t^2}{k_{1t}^2}, \frac{x}{x_1}, \alpha_s \right) \rightarrow \mathcal{K}_{BFKL}^{LL(1/x)} \left(\frac{k_t^2}{k_{1t}^2}, \alpha_s \right). \quad (27)$$

In consequence, we have the linear BFKL equation.

$$\begin{aligned} & -x \frac{\partial F(x, k_t^2)}{\partial x} \\ &= \frac{\alpha_s N_c k_t^2}{\pi} \int_{k_{1t, \min}^2}^{\infty} \frac{dk_{1t}^2}{k_{1t}^2} \left\{ \frac{F(x, k_{1t}^2) - F(x, k_t^2)}{|k_{1t}^2 - k_t^2|} + \frac{F(x, k_t^2)}{\sqrt{k_t^4 + 4k_{1t}^4}} \right\}, \end{aligned} \quad (28)$$

and nonlinear BFKL equation with the modifications of gluon fusion

$$\begin{aligned} & -x \frac{\partial F(x, k_t^2)}{\partial x} \\ &= \frac{\alpha_s N_c k_t^2}{\pi} \int_{k_{1t, \min}^2}^{\infty} \frac{dk_{1t}^2}{k_{1t}^2} \left\{ \frac{F(x, k_{1t}^2) - F(x, k_t^2)}{|k_{1t}^2 - k_t^2|} + \frac{F(x, k_t^2)}{\sqrt{k_t^4 + 4k_{1t}^4}} \right\} \\ & - \frac{36\alpha_s^2}{\pi R^2 k_t^2} \frac{N_c^2}{N_c^2 - 1} \left[\int_{k_{1t, \min}^2}^{k_t^2} \frac{dk_{1t}^2}{k_{1t}^2} F(x, k_{1t}^2) \right]^2 + \frac{18\alpha_s^2}{\pi R^2 k_t^2} \frac{N_c^2}{N_c^2 - 1} \left[\int_{k_{1t, \min}^2}^{k_t^2} \frac{dk_{1t}^2}{k_{1t}^2} F \left(\frac{x}{2}, k_{1t}^2 \right) \right]^2; \\ & -x \frac{\partial F_A(x, k_t^2)}{\partial x} \end{aligned}$$

$$\begin{aligned}
&= \frac{\alpha_s N_c k_t^2}{\pi} \int_{k_{1t,min}^2}^{\infty} \frac{dk_{1t}^2}{k_{1t}^2} \left\{ \frac{F_A(x, k_{1t}^2) - F_A(x, k_t^2)}{|k_{1t}^2 - k_t^2|} + \frac{F_A(x, k_t^2)}{\sqrt{k_t^4 + 4k_{1t}^4}} \right\} \\
&- A^{1/3} \frac{36\alpha_s^2}{\pi R^2 k_t^2} \frac{N_c^2}{N_c^2 - 1} \left[\int_{k_{1t,min}^2}^{k_t^2} \frac{dk_{1t}^2}{k_{1t}^2} F_A(x, k_{1t}^2) \right]^2 + A^{1/3} \frac{18\alpha_s^2}{\pi R^2 k_t^2} \frac{N_c^2}{N_c^2 - 1} \left[\int_{k_{1t,min}^2}^{k_t^2} \frac{dk_{1t}^2}{k_{1t}^2} F_A\left(\frac{x}{2}, k_{1t}^2\right) \right]^2.
\end{aligned} \tag{29}$$

To solve the equations numerically we need to know the mix of the BFKL- and DGLAP-equations. A unified framework which works in all the through (x, k_t) kinematic region was provided by Catani, Ciafaloni, Fiorani and Marchesini (the CCFM equation [49-51]). Based on the coherent radiation of gluons, this equation leads to an angular ordering of the gluon emissions along the chain. In the leading order approximation of $\ln(1/x)$, the CCFM equation reduces to the BFKL equation, whereas at moderate x the angular ordering becomes an ordering in gluon transverse momenta and the CCFM equation becomes equivalent to the standard DGLAP equation.

Unfortunately, in the CCFM schema there contains unknown shadowing and anti-shadowing information in its complicate input distributions. As we know that the BFKL equation can be derived in a dipole picture [52-56]. At large x region ($x > 0.1$), parton densities in nucleon are dilute and the probe interacts with a single parton (Fig.1 a). In this case, the DGLAP dynamics are dominant. At smaller x region ($x < 10^{-3}$), the correlations among the initial partons in a nucleon becomes more important and the dipole configuration dominates the initial state (Fig.1c), and the BFKL dynamics in place of the DGLAP dynamics are dominant. Note that although when $x < 10^{-3}$ the BFKL evolution is dominant according to $\alpha_s \ln(1/x) \sim \mathcal{O}(1)$, we can not exclude directly the BFKL dynamics from the *part* of evolution at a larger x region according to Fig. 1b. A natural connection between two evolution dynamics should be that the BFKL dynamics replace asymptotically the DGLAP dynamics from $x = 0.1$ to 10^{-3} through out the mixing region of the single parton and dipole configuration. Concretely, we take

Equation(21), at $0.15 > x > 10^{-1}$;

Equation(21) $\times [1 - \beta]$ + Equatiuion(29) $\times \beta$, at $10^{-1} > x > 10^{-3}$;

Equation(29), at $x < 10^{-3}$, (30)

where

$$\beta = -\frac{\ln 10}{\ln 10^3 - \ln 10} + \frac{\ln \frac{1}{x}}{\ln 10^3 - \ln 10}. \quad (31)$$

We emphasize that if we use the original form of the GLR-MQ-ZRS equation (13) to replace Eq. (21), the solution of the Eq. (31) becomes very difficult to solve since there exists two different evolution ways.

All the parameters in the solutions of Eqs. (21), (22) and (29) will be determined by the EMC effect. Most of the data about the EMC effect are got by measuring the structure functions. Thus, we should calculate the quark distributions at small x . We assume that the sea quark distributions at the small x range are dominant compared with the gluon distribution, via the DGLAP splitting process $g \rightarrow q\bar{q}$. Thus, the structure function of the deep inelastic process at small x reads [57]

$$\begin{aligned} & F_2(x, Q^2) \\ &= 2 \int_x^1 dx_1 \int^{Q^2} \frac{dk_t^2}{k_t^2} \int^{k_t^2} \frac{dk_{1t}^2}{k_{1t}^2} F\left(\frac{x}{x_1}, k_{1t}^2\right) \sum_q e_q^2 \frac{\alpha_s}{2\pi} P_{qg}(x_1). \end{aligned} \quad (32)$$

where $P_{qg}(x_1)$ is the DGLAP splitting function.

3 The EMC effect

The EMC effect includes the Fermi motion and binding effect at $x > 0.3$ [3]. However, in this work we focus the nuclear shadowing and antishadowing contributions at $x < 0.3$ since we use the RHIC and LHC data at $x \sim k_t/\sqrt{s} < 0.3$.

We choose $x_0 = 0.15$ as the starting point of the evolution in Eqs. (21) and (22), where the nonlinear gluon recombination begins to work. We find that following input is suitable, i.e.,

$$F(2x_0, k_t^2) = 2\sqrt{(k_t^2)} \exp(-(\log(k_t^2))^2). \quad (33)$$

It is necessary to know the value of $F(x_i/2, k_t^2)$ at the step $x = x_i$ in advance to compute Eqs. (21), (22) and (29) numerically. For this sake, we proposed the following program in [58]

$$F\left(\frac{x_i}{2}, k_t^2\right) = F_{Shadowing}\left(\frac{x_i}{2}, k_t^2\right) + \frac{F_{linear}\left(\frac{x_i}{2}, k_t^2\right) - F_{Shadowing}\left(\frac{x_i}{2}, k_t^2\right)}{i\Delta - \Delta + 1}, \quad (34)$$

where $F_{Shadowing}(x_i/2, k_t^2)$ (or $F_{linear}(x_i/2, k_t^2)$) indicates that the evolution from x_i to $x_i/2$ is controlled by Eqs. (21), (22) and (29) without the antishadowing contributions (or is controlled by the linear equation). The parameter $0 < \Delta < 1$, which implies the different velocities approaching to the dynamics of Eqs. (21), (22) and (29).

At first, we use the well known data of $F_{2p}(x, Q^2)$ [59,60] of a free proton in order to determine the parameters in the computations. Then we predict the distributions in nuclei. The dashed curve in Fig. 2 is our fitting result using the input (33), where we take the parameters $R = 2.4 \text{ GeV}^{-1}$, $k_t^2 = 0.01 \text{ GeV}^2$, $\alpha_s = 0.3$ and $\Delta = 0.02$. Note that the contributions of the valence quarks to F_2 at $x > 0.1$ are necessary and they can be parameterized by the difference between the dashed curve and experimental solid curve in Fig.2.

Figure 3 shows our predictions of Eqs. (21), (22) and (29) for the Ca/C, C/Li, Ca/D and Cu/D compared with the EMC and NMC results [61-63]. Their agreement is acceptable.

Different from the scheme of the DGLAP evolution equation, our scheme can predict the nuclear effects for the unintegrated gluon distribution. The results are presented by their ratios of the nuclear unintegrated gluon distributions in Figs.4 and 5. Although deep inelastic scattering experiments do not examine directly these effects, hadron-nucleus scattering at RHIC relates the nuclear unintegrated gluon distributions, which will be used in next section.

Using Eqs. (21), (22) and (29), the ratios of gluon distributions $G_{Ca}(x, Q^2)/G_D(x, Q^2)$ at $Q^2 = 2$ and 10 GeV^2 are given in Fig.6. The curves present a cusps at $x = 0.15$. This is due to a simply assumption in Eq. (12), which leads to the shadowing and antishadowing effects start from $x = 0.15$ and $x = 0.3$, respectively in Eq. (22). One can smear the cusps when considering the gluon fusions with different values of x . However, this will complicate the calculations but doesn't change our following conclusions.

The Q^2 -dependence of the gluon ratio is predicted in the region $10^{-4} < x < 10^{-1}$ in our model. The logarithmic slope b in $G_A/G_{A'} = a + b \ln Q^2$ is positive. However, the corresponding slope in the ratio of the structure functions F_{2Ca}/F_{2D} is negative at small x (see Fig.7). For example, the predicted Q^2 -slope for calcium at $x \simeq 4 \times 10^{-2}$, $b \simeq -0.046$, and at $x \simeq 10^{-2}$, $b \simeq -0.03$, the results are compatible with the measured data in [64].

The data of $G_{Sn}(x, Q^2)/G_C(x, Q^2)$ are measured from inelastic J/ψ production by the NM Collaboration in Ref. [65], which determine a stronger nuclear antishadowing effect but with a larger uncertainty. Our prediction is presented in Fig.8.

Compared with the ESP09 set [27,28], our works predict a more stronger antishadowing effect in the gluon (integrated and unintegrated) distributions of heavy nucleus. One

reasons is that the observed antishadowing effect in the structure functions originates dynamically from the gluon fusions in our model, while in the DGLAP analysis the effect is partly from the input distributions of the valence quarks [27,28]. Another reason is that the A -dependent nonlinear terms enhance the effect of the gluon fusion in the heavy nuclei.

4 The Cronin effect

The Cronin effect is described by the nuclear modification factor R_{dA} , which is defined as the ratio of the number of particles produced in a $d + A$ collision to that in a $p + p$ collision scaled by the number of collisions

$$R_{dA}(k_t) = \frac{\left. \frac{dN_{d-A}(k_t, \eta)}{d^2k_T d\eta} \right|_{\eta=0}}{N_{coll} \left. \frac{dN_{p-p}(k_t, \eta)}{d^2k_t d\eta} \right|_{\eta=0}}, \quad (35)$$

k_t and η are respectively the transverse momentum and the pseudo-rapidity of the observed hadron. N_{coll} is the number of collisions in $d + A$ scattering. In Eq. (35),

$$\begin{aligned} \frac{dN_{p-p}(k_t, \eta)}{d^2k_t d\eta} &= \frac{1}{\sigma_{in}} \frac{d\sigma_{p-p}(k_t, \eta)}{d^2k_t d\eta} \\ &= \frac{1}{\sigma_{in}} \int \frac{dz}{z} J(\eta; k_t; m_{eff}) D_p(z) \delta^2(k_t - zk_{t,g}) \left. \frac{d\sigma_{p-p}(k_{t,g}, y)}{dy d^2k_{t,g}} \right|_{y \rightarrow \eta}, \end{aligned} \quad (36)$$

and

$$\begin{aligned} \frac{1}{N_{coll}} \frac{dN_{d-A}}{d^2k_t d\eta} &= \frac{1}{\sigma_{in}} \frac{d\sigma_{d-A}(k_t, \eta)}{d^2k_t d\eta} \\ &= \frac{1}{\sigma_{in}} \int \frac{dz}{z} J(\eta; k_t; m_{eff}) D_A(z) \delta^2(k_t - zk_{t,g}) \left. \frac{d\sigma_{d-A}(k_{t,g}, y)}{dy d^2k_{t,g}} \right|_{y \rightarrow \eta}, \end{aligned} \quad (37)$$

where $z = k_t/k_{t,g}$; $D_p(z)$ and $D_A(z)$ are the fragmentation functions of gluon jets in proton and nucleus, where the factorized scale-dependence of the fragmentation functions are neglected; The rapidity y of the produced gluon in the center-of-mass frame of $p + p$ collisions is defined by

$$x_{1/2} = \frac{k_{t,g}}{\sqrt{s}} \cdot \exp(\pm y); \quad (38)$$

The relation between the rapidity y and pseudorapidity η of massive particles is

$$y = \frac{1}{2} \ln \left[\frac{\sqrt{\frac{m_{eff}^2 + p_t^2}{p_t^2} + \sinh^2 \eta + \sinh \eta}}{\sqrt{\frac{m_{eff}^2 + p_t^2}{p_t^2} + \sinh^2 \eta - \sinh \eta}} \right], \quad (39)$$

where m_{eff} is the typical invariant mass of the gluon jet.

We assume that the hadrons in the central region are produced from the hadronization of the gluons in $gg \rightarrow g$ mechanism. According to Ref. [34] we have

$$\begin{aligned} & \left. \frac{d\sigma_{p-p}(k_t, \eta)}{d^2k_t d\eta} \right|_{\eta=0} \\ &= \frac{4N_c}{N_c^2 - 1} \int \frac{dz}{z^2} \frac{\alpha_s}{k_{t,g}^2} J^2 D_p(z) \\ & \int^{k_{t,g}^2} dq_{t,g}^2 f_g^p(x, (k_{t,g} - q_{t,g})^2) f_g^p(x, q_{t,g}^2) \Big|_{k_{t,g}=Jk_t/z} \\ & \simeq \frac{4N_c}{N_c^2 - 1} \int \frac{dz}{z^2} \frac{\alpha_s}{k_{t,g}^2} J^2 D_p(z) \\ & \left[f_g^p(x, k_{t,g}^2) G^p(x, k_{t,g}^2) + G^p(x, k_{t,g}^2) f_g^p(x, k_{t,g}^2) \right]_{k_{t,g}=Jk_t/z}, \end{aligned} \quad (40)$$

$$\begin{aligned} & \left. \frac{d\sigma_{d-A}(k_t, \eta)}{d^2k_t d\eta} \right|_{\eta=0} \\ &= \frac{4N_c}{N_c^2 - 1} \int \frac{dz}{z^2} \frac{\alpha_s}{k_{t,g}^2} J^2 D_A(z) \\ & \int^{k_{t,g}^2} dq_{t,g}^2 f_g^p(x, (k_{t,g} - q_{t,g})^2) f_g^A(x, q_{t,g}^2) \Big|_{k_{t,g}=Jk_t/z} \\ & \simeq \frac{4N_c}{N_c^2 - 1} \int \frac{dz}{z^2} \frac{\alpha_s}{k_{t,g}^2} J^2 D_A(z) \\ & \left[f_g^p(x, k_{t,g}^2) G^A(x, k_{t,g}^2) + G^p(x, k_{t,g}^2) f_g^A(x, k_{t,g}^2) \right]_{k_{t,g}=Jk_t/z}, \end{aligned} \quad (41)$$

here we neglect the k_t -dependence in the fragmentation functions.

At the first step, we neglect the interactions at final state, i.e., in Eqs. (40) and (41)

$$D_p(z) = D_A(z) = \delta(z - 1). \quad (42)$$

We indicate this nuclear modification factor as R_{dA}^g , which is drawn in Fig. 9. According to Eq. (38) at $y = 0$ and $\sqrt{s} = 200\text{GeV}$, the antishadowing effect on the gluon jet should distribute in a broad range $8\text{GeV} < k_t < 60\text{GeV}$, which corresponds to the antishadowing range $0.02 < x < 0.3$ in Fig.4.

At the next step, we consider the corrections of the fragmentation functions but neglect the difference between proton and nucleus. We take [66]

$$D_p(z) = D_A(z) = \frac{2}{3} \times 1940z^{1.4}(1-z)^8, \quad (43)$$

where $D(z) \rightarrow 0$ at $z \rightarrow 0$ since the coherence effects in QCD at small z . Our results are plotted with the solid curve in Fig. 10. The data are taken from the BRAHMS results in [6]. One can find that the fragmentation functions shift cross point between the Cronin and anti-Cronin effects towards small k_t , since the position of the peak value of the fragmentation functions always localizes at small z . We find that the nuclear shadowing and antishadowing effects at the initial state dominate the Cronin effect, although a small nuclear modification to the fragmentation functions, i.e., $D_A(z) \neq D_p(z)$ is necessary.

The study on the parton energy loss caused by medium-induced multiple gluon emission in various nuclear conditions is a hot topic, since the data of $Au + Au$ collisions at RHIC show a new hot matter which might be a strongly coupled Quark-Gluon Plasma (sQGP). The presence of a dense medium influences the space-time development of the partonic shower of a jet. When an energetic jet of parton propagates through the medium, a part of its energy transfers to the thermal partons, which is called the parton energy loss. After this jet propagates a long distance in an expanding de-confinement system, most of the gluons carrying the lost energy will escape from the jet cone and will be un-measured. Thus, as an example, the modified fragmentation function in an effective model can be written as [67,68]

$$D_A(z) = \frac{1}{1-\epsilon} D_p\left(\frac{z}{1-\epsilon}\right), \quad (44)$$

where E is the initial energy of a gluon jet and $\epsilon = \Delta E/E$ is fractional energy loss.

We consider a similar energy loss mechanism which exists in $d + Au$ collisions at RHIC but with a smaller value of ϵ . The dashed curve plotted in Fig. 10 is the resulting nuclear suppression factor with $\epsilon = 0.1$. From the results motioned above we find that the anti-Cronin suppression and Cronin enhancement originate from the nuclear shadowing and antishadowing effects in the initial state in the EMC effect.

5 The signals of QGP

One of the important findings at RHIC and LHC is that high transverse momentum hadron production in central heavy ion collisions is suppressed compared with that in (properly scaled) p+p collisions [1, 2]. This suppression is defined as the nuclear suppression factor R_{AA} and can be attributed to energy loss of high- k_t partons that traverse through the hot and dense medium formed in these collisions. However, to extract the energy loss from R_{AA} , it is necessary to have the nuclear effects in the initial parton distributions. Such information can be derived from the integrated and unintegrated gluon distributions in proton and nuclei we obtained.

Several of the most important results obtained at RHIC are related to the high- k_t spectrum in heavy ion $Au + Au$ collisions. In this aspect, a precise determination of the nuclear effects in the initial state of these collisions is fundamental. We present the estimation of the ratio R_{AA} using our parameters in explanation of the EMC- and Cronin-effects

$$R_{AA}(k_t) = \frac{\left. \frac{dN_{A-A}(k_t, \eta)}{d^2k_T d\eta} \right|_{\eta=0}}{N_{coll} \left. \frac{dN_{p-p}(k_t, \eta)}{d^2k_t d\eta} \right|_{\eta=0}}, \quad (45)$$

Firstly we assume that $\epsilon = 0$ in Eq. (44) and calculate the nuclear shadowing and antishadowing effects in the nuclear suppression factor. The result is plotted with the dashed curve in Fig. 11. There exists a big difference between the curve and the data at $k_t > 3\text{GeV}$, which is commonly interpreted in terms of a strong energy loss of the energetic partons when they traverse through a dense medium. For example, we take $\epsilon = 0.4$ (see the dotted curve in Fig. 11). Obviously, a true form of fractional energy loss ϵ has a crossover from a small value of ϵ to a large one when the energy of the gluon jet is increasing. It is interesting that when we take

$$\epsilon = \begin{cases} a & \text{if } E < E_c \\ b & \text{if } E > E_c \end{cases}, \quad (46)$$

where $a = 0.2$ and $b = 0.4$ (i.e., Fig. 12a), we have

$$\begin{aligned} & \left. \frac{d\sigma_{A-A}(k_t, \eta)}{d^2k_t d\eta} \right|_{\eta=0} \\ &= \frac{4N_c}{N_c^2 - 1} \int \frac{dz}{z^2} \frac{\alpha_s}{k_{t,g}^2} J^2 D_A(z) \\ & \int^{k_{t,g}^2} dq_{t,g}^2 f_g^A(x, (k_{t,g} - q_{t,g})^2) f_g^A(x, q_{t,g}^2) \Big|_{k_{t,g}=Jk_t/z} \\ & \simeq \frac{4N_c}{N_c^2 - 1} \int \frac{dz}{z^2} \frac{\alpha_s}{k_{t,g}^2} J^2 D_A(z) \\ & \left[f_g^A(x, k_{t,g}^2) G^A(x, k_{t,g}^2) + G^A(x, k_{t,g}^2) f_g^A(x, k_{t,g}^2) \right]_{k_{t,g}=Jk_t/z}, \end{aligned} \quad (47)$$

$$\begin{aligned} & \left. \frac{d\sigma_{A-A}(k_t, \eta)}{d^2k_t d\eta} \right|_{\eta=0} \\ &= \frac{4N_c}{N_c^2 - 1} \int_0^{k_t/E_c} \frac{dz}{z^2} \frac{\alpha_s}{k_{t,g}^2} J^2 D_A(z) \left[f_g^A(x, k_{t,g}^2) G^A(x, k_{t,g}^2) + G^A(x, k_{t,g}^2) f_g^A(x, k_{t,g}^2) \right]_{k_{t,g}=Jk_t/z} \\ & + \frac{4N_c}{N_c^2 - 1} \int_{k_t/E_c}^{1-b} \frac{dz}{z^2} \frac{\alpha_s}{k_{t,g}^2} J^2 D_A(z) \left[f_g^A(x, k_{t,g}^2) G^A(x, k_{t,g}^2) + G^A(x, k_{t,g}^2) f_g^A(x, k_{t,g}^2) \right]_{k_{t,g}=Jk_t/z} \\ & \quad \text{if } k_t < E_c(1-b); \\ &= \frac{4N_c}{N_c^2 - 1} \int_0^{1-a} \frac{dz}{z^2} \frac{\alpha_s}{k_{t,g}^2} J^2 D_A(z) \left[f_g^A(x, k_{t,g}^2) G^A(x, k_{t,g}^2) + G^A(x, k_{t,g}^2) f_g^A(x, k_{t,g}^2) \right]_{k_{t,g}=Jk_t/z} \\ & + \frac{4N_c}{N_c^2 - 1} \int_{k_t/E_c}^{1-b} \frac{dz}{z^2} \frac{\alpha_s}{k_{t,g}^2} J^2 D_A(z) \left[f_g^A(x, k_{t,g}^2) G^A(x, k_{t,g}^2) + G^A(x, k_{t,g}^2) f_g^A(x, k_{t,g}^2) \right]_{k_{t,g}=Jk_t/z} \\ & \quad \text{if } E_c(1-b) < k_t < E_c(1-a); \\ &= \frac{4N_c}{N_c^2 - 1} \int_0^{1-a} \frac{dz}{z^2} \frac{\alpha_s}{k_{t,g}^2} J^2 D_A(z) \left[f_g^A(x, k_{t,g}^2) G^A(x, k_{t,g}^2) + G^A(x, k_{t,g}^2) f_g^A(x, k_{t,g}^2) \right]_{k_{t,g}=Jk_t/z} \\ & \quad \text{if } k_t > E_c(1-a). \end{aligned} \quad (48)$$

we find that the resulting solid curve plotted in Fig. 11 consists with the experiment data at $1\text{GeV} < k_t < 10\text{GeV}$.

Recently, the nuclear modification factor in central $Pb+Pb$ collisions at $\sqrt{s} = 2.76TeV$ is published by the ALICE Collaboration at LHC [2]. The data indicate that R_{AA} reaches a minimum at $k_t = 6 - 7GeV$, which is about 0.14 and smaller than that at RHIC. However, it rises steeply the asymptotic value of RHIC at large k_t . Therefore, it is unclear whether a more dense matter is formed or not at LHC. Obviously, it is necessary to determinate quantitatively the energy loss after gluon shadowing and antishadowing effects are excluded. For this sake, similar to the above approach, we take $a = 0$ and $b = 0.58$ (Fig. 12b) in Eq. (46) and plot the result with the solid curve in Fig. 13. The dashed and pointed curves are plotted respectively when $\epsilon = 0$ and 0.58. Equation (46) is a good approximation to describe the nuclear suppression factor at $1GeV < k_t < 10GeV$ although the results show that the energy loss ϵ decrease with the jet energy $E \gg 10 GeV$. Thus, a rapid crossover from weak energy loss to strong energy loss at a universal critical energy of gluon jet $E_c \sim 10GeV$ is found.

Finally, we discuss the contributions of the BFKL-corrections. When Eq. (29) is neglected, it is found that the BFKL-corrections to the ratios R_{dA} and R_{AA} can be neglected in the present energy scale.

In summary, the EMC- and Cronin-effects are explained by a unitarized evolution equation, where the shadowing and antishadowing corrections are dynamically produced by gluon fusions. An alternative form of the GLR-MQ-ZRS equation is derived. The resulting integrated and unintegrated gluon distributions in proton and nuclei are used to analyze the contributions of the initial parton distributions to the nuclear suppression factor in heavy ion collisions. A simulation of the fractional energy loss is extracted from the data at RHIC and LHC, where the contributions of the nuclear shadowing and antishadowing effects are considered. A rapid crossover from weak energy loss to strong energy loss is found at a universal critical energy of gluon jet $E_c \sim 10GeV$.

Acknowledgments: This work was supported in part by the National Natural Science Foundations of China (under Grants No. 10875044 and No. 11205227) and the Project of Knowledge Innovation Program (PKIP) of Chinese Academy of Sciences, Grant No. KJCX2.YW.W10

Appendix. GLR-MQ-ZRS equation: The modifications of the gluon recombination to the DGLAP evolution in the GLR-MQ-ZRS equation has following form [38-40], which work in whole x range .

$$\begin{aligned}
& \frac{dG(x, Q^2)}{d \ln Q^2} \\
&= P_{gg}^{AP} \otimes G(x, Q^2) + P_{gq}^{AP} \otimes S(x, Q^2) \\
&- 2 \int_x^{1/2} \frac{dx_1}{x_1} \frac{x}{x_1} \mathcal{K}_{GLR-MQ-ZRS}^{GG \rightarrow GG, LL(Q^2)} \left(\frac{x}{x_1}, \alpha_s \right) G^{(2)}(x_1, \mu_1^2) \\
&+ \int_{x/2}^{1/2} \frac{dx_1}{x_1} \frac{x}{x_1} \mathcal{K}_{GLR-MQ-ZRS}^{GG \rightarrow GG, LL(Q^2)} \left(\frac{x}{x_1}, \alpha_s \right) G^{(2)}(x_1, \mu_1^2), \tag{A-1}
\end{aligned}$$

for gluon distribution and

$$\begin{aligned}
& \frac{dxS(x, Q^2)}{d \ln Q^2} \\
&= P_{qg}^{AP} \otimes G(x, Q^2) + P_{qq}^{AP} \otimes S(x, Q^2) \\
&- 2 \int_x^{1/2} \frac{dx_1}{x_1} \frac{x}{x_1} \mathcal{K}_{GLR-MQ-ZRS}^{GG \rightarrow S\bar{S}, LL(Q^2)} \left(\frac{x}{x_1}, \alpha_s \right) G^{(2)}(x_1, \mu_1^2) \\
&+ \int_{x/2}^{1/2} \frac{dx_1}{x_1} \frac{x}{x_1} \mathcal{K}_{GLR-MQ-ZRS}^{GG \rightarrow S\bar{S}, LL(Q^2)} \left(\frac{x}{x_1}, \alpha_s \right) G^{(2)}(x_1, \mu_1^2), \tag{A-2}
\end{aligned}$$

for sea quark distributions, where P^{AP} are the evolution kernels of the linear DGLAP equation and the recombination functions

$$\begin{aligned}
& \frac{dx_1}{x_1} \mathcal{K}_{GLR-MQ-ZRS}^{GG \rightarrow GG, LL(Q^2)} \\
&= \frac{9\alpha_s^2 (2x_1 - x)(72x_1^4 - 48x_1^3x + 140x_1^2x^2 - 116x_1x^3 + 29x^4)}{64 x_1^5} dx_1 \tag{A-3}
\end{aligned}$$

$$\begin{aligned}
& \frac{dx_1}{x_1} \mathcal{K}_{GLR-MQ-ZRS}^{GG \rightarrow S\bar{S}, LL(Q^2)} \\
&= \frac{\alpha_s^2 (2x_1 - x)^2 (18x_1^2 - 21x_1x + 14x)}{48 x_1^5} dx_1 \tag{A-4}
\end{aligned}$$

References

- [1] K. Adcox et al. (PHENIX Collaboration), Suppression of Hadrons with Large Transverse Momentum in Central Au+Au Collisions at $\sqrt{S_{NN}} = 130$ GeV, Phys. Rev. Lett. **88** (2002) 022301.
- [2] K. Aamodt, et al. [ALICE Collaboration], Suppression of charged particle production at large transverse momentum in central Pb–Pb collisions at $\sqrt{S_{NN}} = 2.76$ TeV, arXiv:1012.1004.
- [3] M. Arneodo, Nuclear effects in structure functions, Phys. Rep. **240** (1994) 301.
- [4] N.N. Nikolaev and V.I. Zakharov, Parton model and deep inelastic scattering on nuclei, Phys. Lett. **B55** (1975) 397.
- [5] J. W. Cronin, H. J. Frisch, M. J. Shochet, J. P. Boymond, R. Mermod, P. A. Piroue and R. L. Sumner, Production of hadrons at large transverse momentum at 200, 300, and 400 GeV, Phys. Rev. **D11** (1975) 3105.
- [6] B. B. Back et al. [PHOBOS Collaboration], Centrality Dependence of Charged-Hadron Transverse-Momentum Spectra in d+Au Collisions at $\sqrt{S_{NN}} = 200$ GeV, Phys. Rev. Lett. **91** (2003) 072302.
- [7] S. S. Adler et al. [PHENIX Collaboration], Absence of Suppression in Particle Production at Large Transverse Momentum in $\sqrt{S_{NN}} = 200$ GeV d+Au Collisions , Phys. Rev. Lett. **91** (2003) 072303.
- [8] J. Adams et al. [STAR Collaboration], Evidence from d+Au Measurements for Final-State Suppression of High- p_T Hadrons in Au+Au Collisions at RHIC, Phys. Rev. Lett. **91**, (2003) 072304.

- [9] I. Arsene et al. [BRAHMS Collaboration], Transverse-Momentum Spectra in Au+Au and d+Au Collisions at $\sqrt{S_{NN}} = 200$ GeV and the Pseudorapidity Dependence of High- p_T Suppression, Phys. Rev. Lett. **91** (2003) 072305.
- [10] J.Jalilian-Marian, A. Kovner, L. McLerran and H. Weigert, The Intrinsic glue distribution at very small x, Phys. Rev. **D55** (1997) 5414.
- [11] J.Jalilian-Marian, A. Kovner, A. Leonidov and H. Weigert, The BFKL equation from the Wilson renormalization group, Nucl. Phys. **B504** (1997) 415.
- [12] J.Jalilian-Marian, A. Kovner, A. Leonidov and H. Weigert, The Wilson renormalization group for low x physics: Towards the high density regime, Phys. Rev. **D59** (1999) 014014.
- [13] H. Weigert, Unitarity at small Bjorken x, Nucl. Phys. **A703** (2002) 823.
- [14] E. Iancu, A. Leonidiv and L. McLerran, Nonlinear gluon evolution in the color glass condensate, Nucl. Phys. **A692** (2001) 583.
- [15] E. Iancu, A. Leonidiv and L. McLerran, The Renormalization group equation for the color glass condensate, Phys. Lett. **B510** (2001) 133.
- [16] W. Zhu, D.L. Xue, K.M. Chai and Z.X. Xu, Antishadowing contribution to the small x behavior of the gluon distribution, Phys. Lett. **B317** (1993) 200.
- [17] W. Zhu, K.M. Chai and B. He, Antishadowing properties in the small-x region, Nucl. Phys. **B427** (1994) 525.
- [18] W. Zhu, K.M. Chai and B. He, Predictions for the low-x structure function in the modified GLR equation, Nucl. Phys. **B449** (1995) 183.

- [19] F. Gelis and J. Jalilian-Marian, From deep inelastic scattering to proton-nucleus collisions in the color glass condensate model, *Phys. Rev.* **D67** (2003) 074019.
- [20] E. Iancu, K. Itakura, D. N. Triantafyllopoulos, Cronin effect and high- p_{\perp} suppression in the nuclear gluon distribution at small x , *Nucl.Phys.* **A742** (2004) 182.
- [21] D. Kharzeev, Y. V. Kovchegov, K. Tuchin, Nuclear modification factor in d+Au collisions: onset of suppression in the color glass condensate, *Phys.Lett.* **B599** (2005) 23.
- [22] E. Cattaruzza, D. Treleani, Cronin Effect And Energy Conservation Constraint In pA Collisions At LHC And RHIC, *Acta Phys. Polon.* **B36** (2005) 575.
- [23] A. H. Mueller, Small- x behavior and parton saturation: A QCD model, *Nucl. Phys.* **B335** (1990) 115.
- [24] L. D. McLerran and R. Venugopalan, Computing quark and gluon distribution functions for very large nuclei, *Phys. Rev.* **D49** (1994) 2233.
- [25] L. D. McLerran and R. Venugopalan, Gluon distribution functions for very large nuclei at small transverse momentum, *Phys. Rev.* **D49** (1994) 3352.
- [26] J. L. Albacete, N. Armesto, A. Kovner, C. A. Salgado, U. A. Wiedemann, Energy Dependence of the Cronin Effect from Nonlinear QCD Evolution, *Phys. Rev. Lett.* **92** (2004) 082001.
- [27] K. J. Eskola, H. Paukkunen, C. A. Salgado, An improved global analysis of nuclear parton distribution functions including RHIC data, *JHEP* **0807** (2008) 102.
- [28] K. J. Eskola, H. Paukkunen, C. A. Salgado, EPS09 – A new generation of NLO and LO nuclear parton distribution functions, *JHEP* **0904** (2009) 65.

- [29] G. Altarelli and G. Parisi, Asymptotic Freedom in Parton Language, Nucl. Phys. **B126** (1977) 298.
- [30] V.N. Gribov and L.N. Lipatov, Deep inelastic e–p scattering in perturbation theory, Sov. J. of Nucl. Phys. **15** (1972) 438.
- [31] Yu.L. Dokshitzer, Calculation of the Structure Functions for Deep Inelastic Scattering and $e^+ e^-$ Annihilation by Perturbation Theory in Quantum Chromodynamics, JETP **46** (1977) 641.
- [32] E.R. Cazaroto, F. Carvalho, V.P. Goncalves, F.S. Navarra, Straining the nuclear gluon distribution in eA processes at RHIC, Phys. Lett. **B669** (2008) 331.
- [33] C. Brenner Mariotto, V. P. Goncalves, Nuclear shadowing and prompt photons in hadronic collisions at ultrarelativistic energies, Phys. Rev. **C78** (2008) 037901.
- [34] L.V. Gribov, E.M. Levin and M.G. Ryskin, Semihard processes in QCD, Phys. Rep. **100** (1983) 1.
- [35] A.H. Mueller and J. Qiu, Gluon recombination and shadowing at small values of x , Nucl. Phys. **B268** (1986) 427.
- [36] K.J. Eskola, J.W. Qiu and X.N. Wang, Perturbative gluon shadowing in heavy nuclei, Phys. Rev. Lett. **72** (1994) 36.
- [37] K.J. Eskola, H. Honkanen, V.J. Kolhinen, J.W. Qiu and C.A. Salgado, Nonlinear corrections to the DGLAP equations in view of the HERA data, Nucl. Phys. **B660** (2003) 211.
- [38] W. Zhu, A New approach to parton recombination in a QCD evolution equation, Nucl. Phys. **B551** (1999) 245.

- [39] W. Zhu and J.H.Ruan, A new modified Altarelli-Parisi evolution equation with parton recombination in proton, Nucl. Phys. **B559** (1999) 378.
- [40] W. Zhu and Z.Q. Shen, Properties of Parton Recombination function, High Energy Physics and Nuclear Physics, **29** (2005) 109.
- [41] J. Kogut and L. Susskind, Scale-invariant parton model, Phys. Rev. **D9** (1974) 697.
- [42] J.H. Ruan and W. Zhu, Prediction for unintegrated parton distributions, Phys. Rev. **C80** (2009) 045209.
- [43] L.N. Lipatov, Reggeization of the Vector Meson and the Vacuum Singularity in Non-abelian Gauge Theories, Sov. J. of Nucl. Phys. **23** (1976) 338.
- [44] V. S. Fadin, E.A. Kuraev and L.N. Lipatov, On the Pomernanchuk Singularity in Asymptotically Free Theories, Phys. Lett. **B60** (1975) 50.
- [45] E.A. Kuraev, L.N. Lipatov and V. S. Fadin, Multi - Reggeon Processes in the Yang-Mills Theory, JETP, **44** (1976) 443.
- [46] E.A. Kuraev, L.N. Lipatov and V. S. Fadin, The Pomernanchuk Singularity in Non-abelian Gauge Theories, JETP, **45** (1977) 199.
- [47] I. I. Balitsky and L.N. Lipatov, The Pomernanchuk Singularity in Quantum Chromodynamics, Sov. J. of Nucl. Phys. **28** (1976) 822.
- [48] I. I. Balitsky and L.N. Lipatov, Calculation Of Meson Meson Interaction Cross-Section In Quantum Chromodynamics, JETP Letter, **30** (1979) 355.
- [49] M. Ciafaloni, Coherence effects in initial jets at small Q^2/s , Nucl. Phys. **B296** (1988)

- [50] S. Catani, F. Fiorani and G. Marchesini, QCD coherence in initial state radiation, Phys. Lett. **B234** (1990) 339.
- [51] S. Catani, F. Fiorani and G. Marchesini, Small- x behaviour of initial state radiation in perturbative QCD, Nucl. Phys. **B336** (1990) 18.
- [52] N.N. Nikolaev and B.G. Zakharov, Color transparency and scaling properties of nuclear shadowing in deep inelastic scattering, Zei. fur Phys. **49** (1991) 607.
- [53] A. H. Mueller, Soft gluons in the infinite momentum wave function and the BFKL pomeron, Nucl. Phys. **B415** (1994) 373.
- [54] A. H. Mueller and B. Patel, Single and double BFKL pomeron exchange and a dipole picture of high-energy hard processes, Nucl. Phys. **B425** (1994) 471.
- [55] A. H. Mueller, Unitarity and the BFKL pomeron, Nucl. Phys. **B437** (1995) 107.
- [56] W. Zhu, Z.Q. Shen and J.H.Ruan, A New Perspective on Gluon Distribution at Small x , hep-ph/0703309.
- [57] A.J. Askew, J. Kwiecinski, A.D. Martin and P.J. Sutton, QCD predictions for deep-inelastic structure functions at the DESY ep collider HERA, Phys. Rev. **D47** (1993) 3775.
- [58] W. Zhu, J.H. Ruan, J.F. Yang and Z.Q. Shen, Contributions of gluon recombination to saturation phenomena, Phys. Rev. **D68** (2003) 094015.
- [59] M.Derrick et al, Measurement of the F_2 structure function in deep inelastic e+p scattering using 1994 data from the ZEUS detector at HERA, Zeit.Phys. **C72** (1996) 399.

- [60] A.C.Benvenuti et al., A high statistics measurement of the proton structure functions $F^2(x, Q^2)$ and R from deep inelastic muon scattering at high Q^2 , Phys.Lett. **B223** (1989) 485.
- [61] CERN NA28/EMC, M. Arneodo et al., Shadowing in deep inelastic muon scattering from nuclear targets, Phys. Lett. **B211** (1988) 493.
- [62] CERN NA28/EMC, M. Arneodo et al., Measurements of the nucleon structure function in the range $0.002 < x < 0.17$ and $0.2 < Q^2 < 8 \text{ GeV}^2$ in deuterium, carbon and calcium, Nucl. Phys. **B333** (1990) 1.
- [63] CERN NA37/NMC, P. Amaudruz et al., A re-evaluation of the nuclear structure function ratios for D, He, ${}^6\text{Li}$, C and Ca, Nucl. Phys. **B441** (1995) 3.
- [64] A. Bodek (SLAC E139), talk at the Lepton-Photon Symposium and Europhysics Conference on High Energy Physics LP-HEP91, Geneva, Switzerland, 25th July-1st August 1991.
- [65] CERN NA37/NMC, P. Amaudruz et al., Ratio of J/ψ production cross sections in deep inelastic muon scattering from tin and carbon, Nucl. Phys. **B371** (1992) 553.
- [66] M. Hirai, S. Kumano, T. H. Nagai and K. Sudoh, Determination of fragmentation functions and their uncertainties, Phys. Rev. **D75** (2007) 094009.
- [67] X. N. Wang, Z. Huang and I. Sarcevic, Jet Quenching in the Direction Opposite to a Tagged Photon in High-Energy Heavy-Ion Collisions, Phys. Rev. Lett. **77** (1996) 231.
- [68] X. N. Wang and Z. Huang, Medium-induced parton energy loss in $\gamma+$ jet events of high-energy heavy-ion collisions, Phys. Rev. **C55** (1997) 3047.

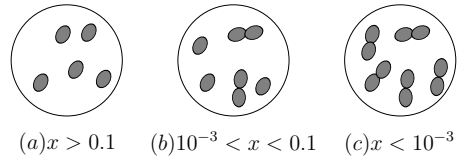


Fig. 1 The kinematic regions of the DGLAP- and BFKL equations.

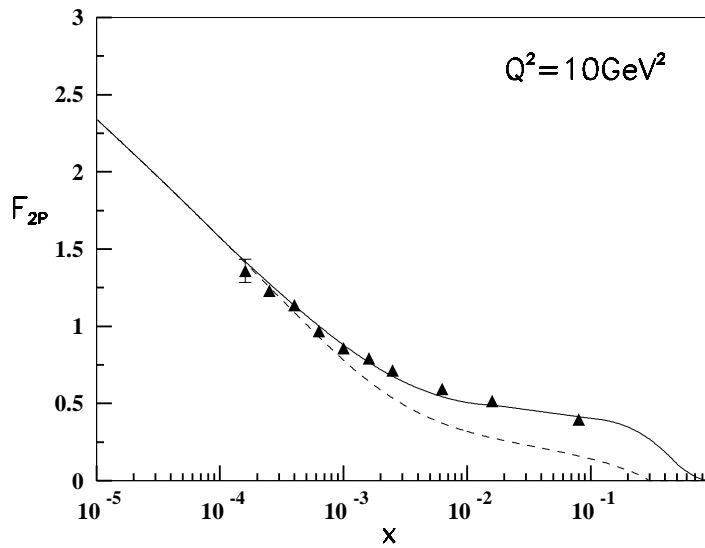


Fig. 2 The fit of the computed $F_{2P}(x, Q^2 = 10 \text{ GeV}^2)$ in proton by the evolution equations (21), (29) and (32) using the input Eq. (33) (dashed curve). The contributions of the valence quarks are parameterized by the differences between solid and dashed curves. The data are taken from Ref. [58].

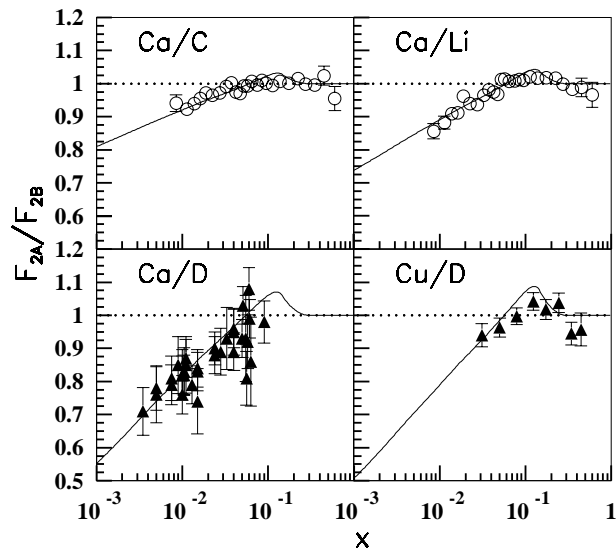


Fig. 3 Predictions of the evolution equations (21), (22) and (29) compared with the EMC ratio of the structure functions for various nuclei. The data are taken from [59-62]. All curves are for $Q^2 = 10 \text{ GeV}^2$.

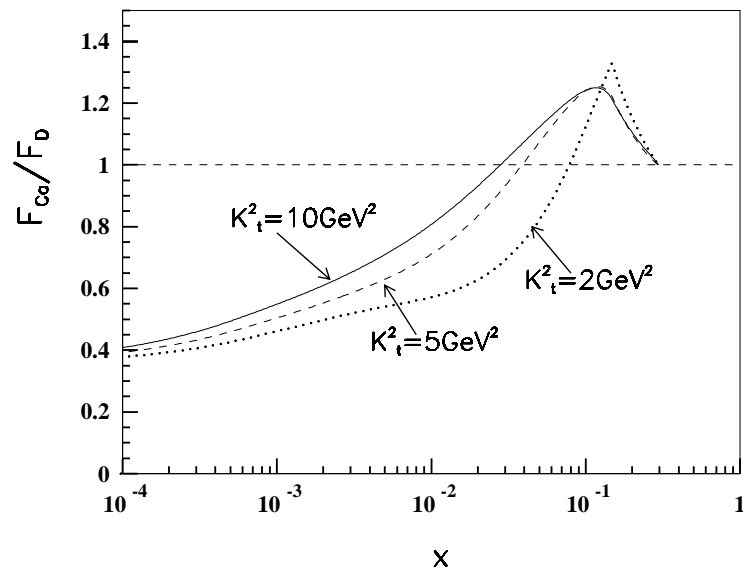


Fig. 4 Predictions of the evolution equations (21), (22) and (29) for the ratio of the unintegrated gluon distributions in Ca/D with different values of x and given k_t .

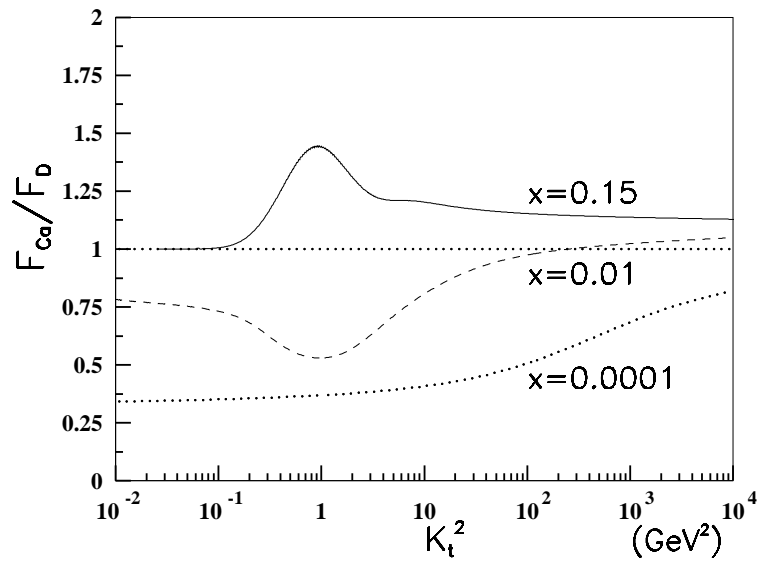


Fig. 5 Similar to Fig. 4 but with different values of k_t and given x .

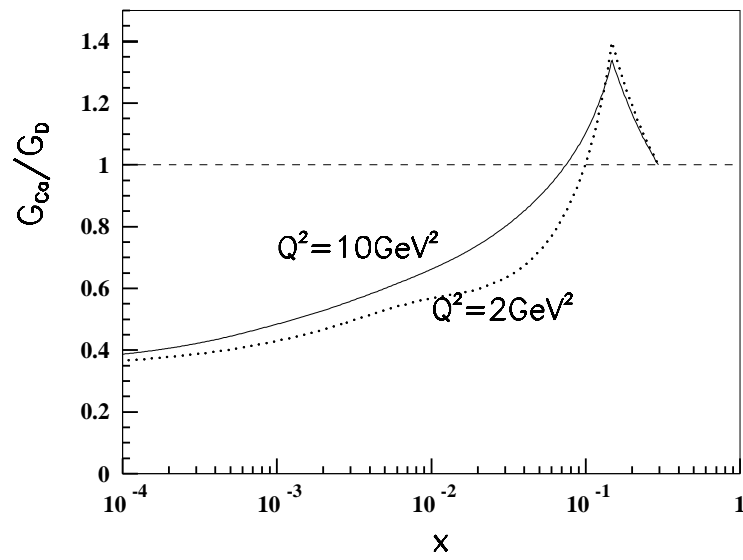


Fig. 6 x -dependence of the ratio for the integrated gluon distributions in Ca/D with the evolution equations (21), (22) and (29).

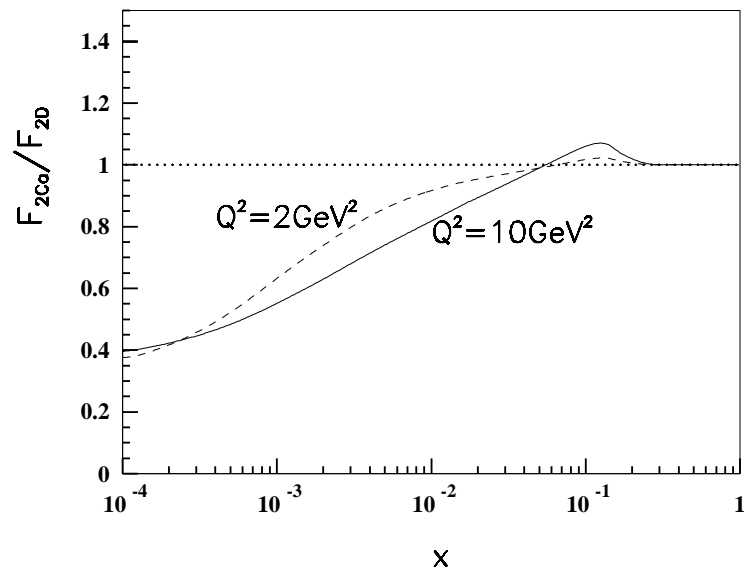


Fig. 7 Similar to Fig. 6 but for the the ratio of the structure functions.

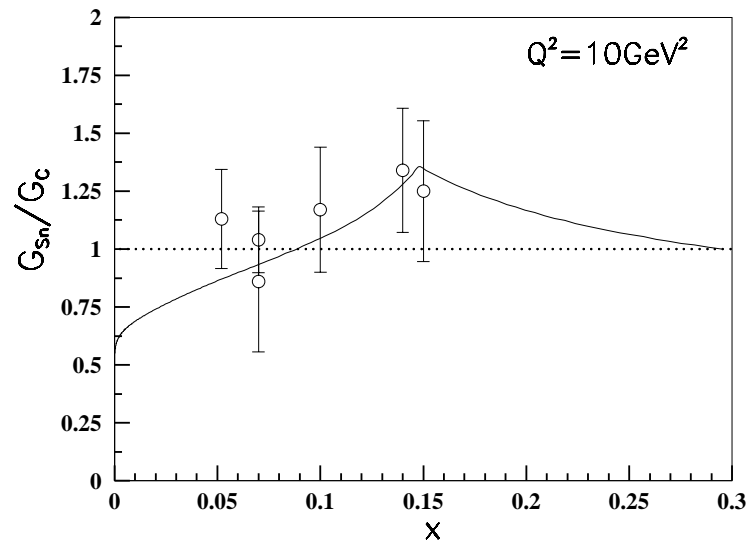


Fig. 8 Predictions for the ratio of the gluon distributions in Sn/C and the data are taken from Ref. [64].

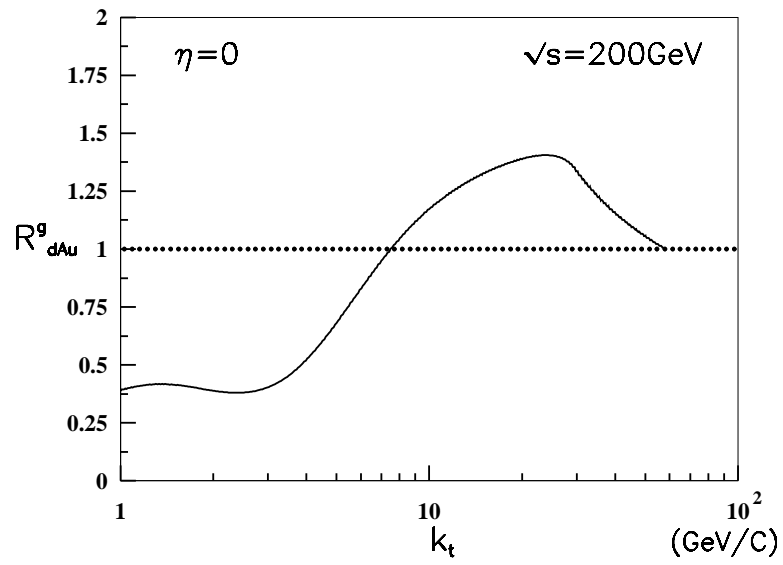


Fig. 9 Predicted nuclear modification factor R_{dAu}^g of gluon jet in central $d + Au$ collisions at $\sqrt{s} = 200\text{GeV}$.

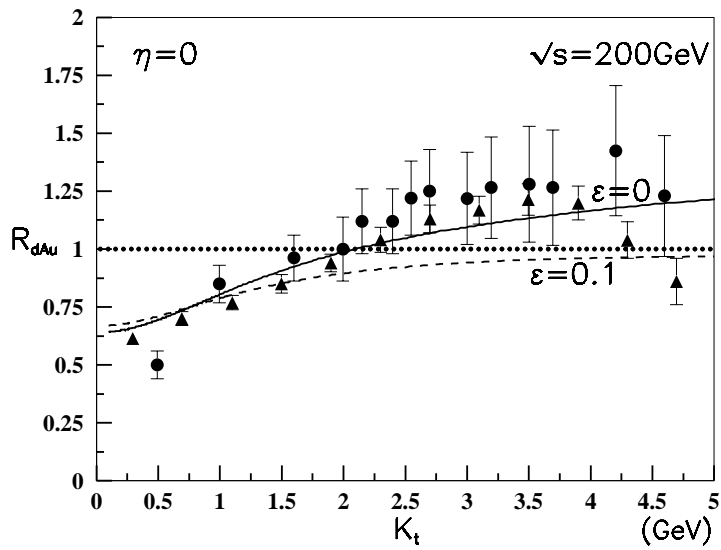


Fig. 10 Nuclear modification factor R_{dAu} of charged particles in central $d+Au$ collisions at $\sqrt{s} = 200\text{GeV}$, where fractional energy loss $\epsilon = 0$ (solid curve) and 0.1 (dashed curve). The data are taken from Ref. [1].

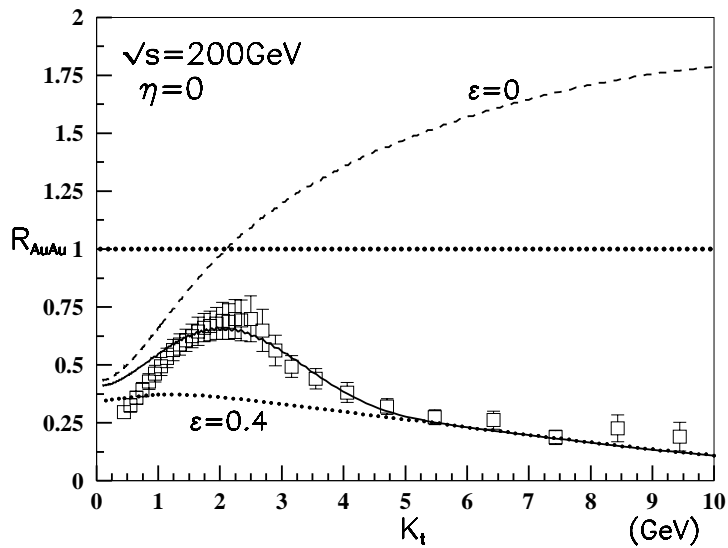


Fig. 11 Estimated nuclear suppression factor R_{AA} in central $Au + Au$ collisions at $\sqrt{s} = 200\text{GeV}$: solid curve using Eq. 46 with $a = 0.2$, $b = 0.4$, (see Fig. 12a); dashed curve using $\epsilon = 0$, and pointed curve using $\epsilon = 0.4$. The data are taken from Ref. [1].

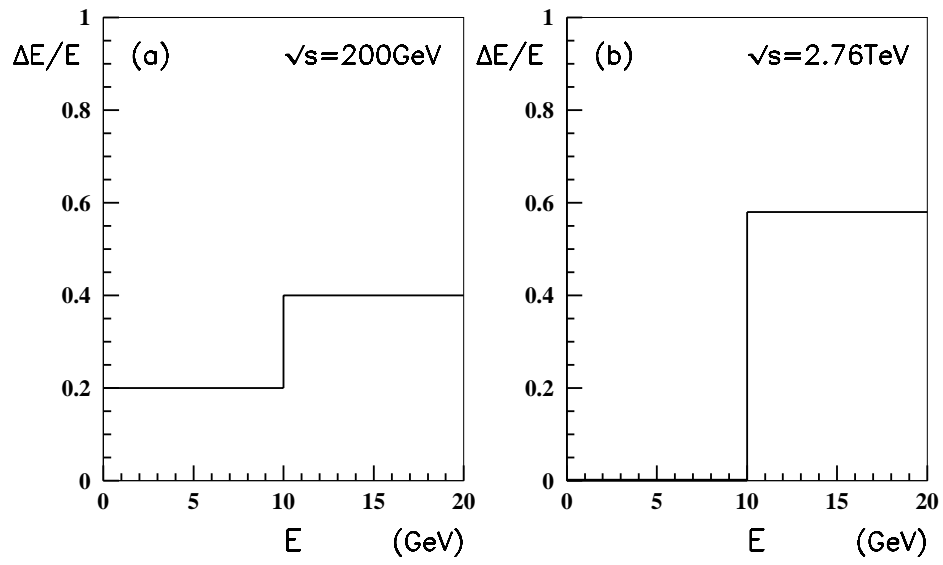


Fig. 12 Two possible fractional energy losses, which correspond to (a) central collisions at $\sqrt{s} = 200\text{GeV}$ for $Au + Au$ and (b) at $\sqrt{s} = 2.76\text{TeV}$ for $Pb + Pb$, respectively.

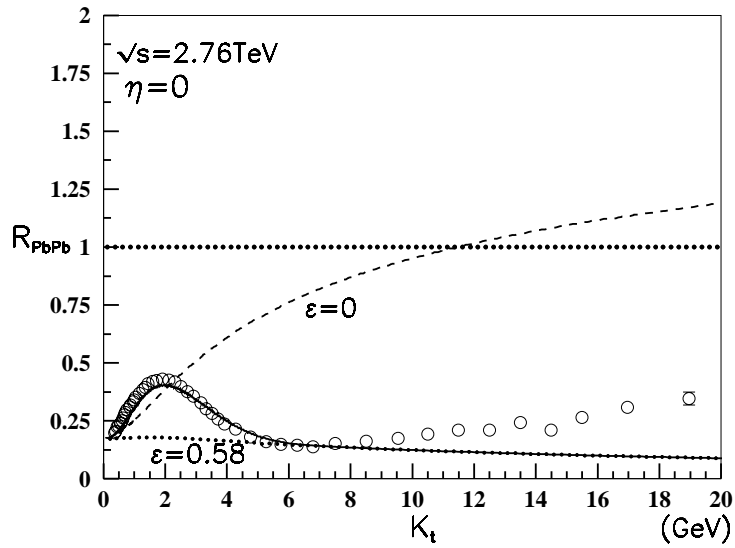


Fig. 13 Similar to Fig. 11, but for central $Pb + Pb$ collisions at $\sqrt{s} = 2.76\text{TeV}$, where solid curve using Eq. 46 with $a = 0$, $b = 0.58$, (see Fig. 12b); dashed curve using $\epsilon = 0$, and pointed curve using $\epsilon = 0.58$. The data are taken from Ref. [2].